

Article

Technological Prospects of Biochar Derived from Viticulture Waste: Characterization and Application Perspectives

Veronica D'Eusanio ^{1,2,*} , Antonio Lezza ¹, Biagio Anderlini ¹ , Daniele Malferrari ¹ , Marcello Romagnoli ^{3,4} 
and Fabrizio Roncaglia ^{1,2,3,*} 

¹ Department of Chemical and Geological Sciences, University of Modena and Reggio Emilia, 41125 Modena, Italy; antonio.lezza@unimore.it (A.L.); biagio.anderlini@unimore.it (B.A.); daniele.malferrari@unimore.it (D.M.)

² National Interuniversity Consortium of Materials Science and Technology (INSTM), 50121 Firenze, Italy

³ Interdepartmental Centre H2-MORE, University of Modena and Reggio Emilia, Via Università 4, 41121 Modena, Italy; marcello.romagnoli@unimore.it

⁴ Department of Engineering "Enzo Ferrari", University of Modena and Reggio Emilia, Via Vivarelli 10, 41125 Modena, Italy

* Correspondence: veronica.deusanio@unimore.it (V.D.); fabrizio.roncaglia@unimore.it (F.R.)

Abstract: The increasing demand for sustainable agricultural practices aimed at reducing carbon dioxide emissions has driven the exploration of converting viticulture residues into biochar. This study investigates the potential technological applications of biochar as a filler for the production of electrically conductive composite materials, suitable to Bipolar Plate (BP) manufacturing. Grape seeds (GSs), defatted grape seeds (DGSs), wood stems (WSs), and whole grape seeds (WGSs) were converted into biochar samples through low-temperature (300 °C) pyrolysis for 3 or 24 h. The composition and thermal stability of biochar were evaluated through thermogravimetric analysis (TG), which provided valuable insights into interpreting the in-plane conductivity (IPC) values of the BP samples. Pyrolyzed GS and DGS biochar samples demonstrated enhanced thermal stability and conferred higher IPC values compared to WS counterparts. This indicates a clear correlation between the formation of carbon-rich structures during pyrolysis and overall electrical conductivity. In contrast, pyrolyzed WGSs produced BP samples with lower IPC values due to the presence of lipids, which were not effectively degraded by the low-temperature pyrolysis.

Keywords: biochar; biomass pyrolysis; viticulture waste; TGA; electro-conductive materials



Citation: D'Eusanio, V.; Lezza, A.; Anderlini, B.; Malferrari, D.; Romagnoli, M.; Roncaglia, F. Technological Prospects of Biochar Derived from Viticulture Waste: Characterization and Application Perspectives. *Energies* **2024**, *17*, 3421. <https://doi.org/10.3390/en17143421>

Academic Editors: Marcin Sajdak, Roksana Muzyka and Grzegorz Gałko

Received: 14 June 2024
Revised: 1 July 2024
Accepted: 10 July 2024
Published: 11 July 2024



Copyright: © 2024 by the authors. Licensee MDPI, Basel, Switzerland. This article is an open access article distributed under the terms and conditions of the Creative Commons Attribution (CC BY) license (<https://creativecommons.org/licenses/by/4.0/>).

1. Introduction

Wine production, deeply rooted in the cultural fabric of Europe, is a fundamental pillar of social, commercial, and economic life in major producing countries such as Italy, France, and Spain. The wine industry in Italy, for instance, boasts a significant output, producing approximately 5.1 million tonnes of wine and 8.1 million tonnes of grapes in 2021 alone [1]. However, this substantial production volume also generates considerable waste. Vinification processes inherently produce byproducts such as grape pomace, lees, and residues from cleaning agents and chemicals used in the production process. Grape pomace, mainly composed of skins, seeds, and some stems, generally accounts for ~20–30% (*w/w*) of the original grape weight [2]. Managing these byproducts poses environmental challenges, as improper disposal or treatment can lead to pollution and ecosystem degradation. For instance, incineration or landfilling can result in adverse environmental consequences, including surface and groundwater pollution, CO₂ emissions, attraction of agricultural pests and flies, and the production of unpleasant odors [2–4].

The considerable amounts of waste byproducts suggest the importance of devising strategies aimed at minimizing the environmental impact within the wine industry. This necessitates a focus on circular-economy principles, wherein high-value byproducts are

effectively utilized to create additional value and reduced waste. Examples of such practices include the extraction of grape seed oil or polyphenols and conversion into biofuels. These approaches not only contribute to waste reduction but also offer economic and environmental benefits to wineries, aligning with sustainability principles in viticulture and oenology. In pursuit of zero waste in the viticulture sector, converting solid residues from grape pomace into biochar through pyrolysis represents a promising option [2,5]. This approach offers several advantages, including the potential to incorporate secondary waste generated from previous extractions, such as defatted grape seeds, as well as waste materials devoid of significant extractable components, such as woody stems or canes.

The pyrolysis process is easily implemented but intrinsically complex, involving diverse and interrelated physical and chemical transformations that result in the production of numerous volatile and non-volatile species [6]. Several process parameters, such as residence time, heating rate, and feedstock composition [7], influence the yield and morphology of the obtained biochar. However, pyrolysis temperature remains the most important parameter [8]. The characteristics of the obtained biochar also depend significantly on the specific biomass substrate, solid-volume-to-surface-area ratio, and moisture content [9]. The explicit quantities of cellulose, hemicellulose, and lignin in the biomass significantly influence the nature and yield of pyrolysis products. For instance, cellulose tends to produce more volatile organic compounds (VOCs) and tars, whereas lignin contributes to the formation of char and aromatic compounds. Additionally, the presence of proteins and lipids within the biomass leads to the formation of nitrogen- and oxygen-containing compounds. The moisture content of the biomass also plays a crucial role, affecting the thermal degradation pathways and the overall energy efficiency of the process. Other factors, such as the presence of minerals and inorganic elements, further modulate the pyrolysis reactions and the quality of the resulting bio-oil, gas, and biochar.

Several studies have highlighted the potential of biochar production from biomass via slow pyrolysis, detecting an annual net energy production ranging from 26,008 to 49,903 MJ/ha in the form of syngas [5]. The energy yield from syngas ranges between 2 and 7 MJ/MJ, surpassing the energy output of ethanol production, which typically ranges from 0.7 to 2.2 MJ/MJ [10,11]. Furthermore, biochar production yields substantial heat, offering opportunities to reduce reliance on fossil fuels. Beyond energy benefits, the conversion of biomass into biochar holds promise in mitigating net greenhouse gas emissions [12], improving soil properties [13], and acting as a remediation agent for wastewater contaminants [14–16], thus underscoring its potential as an environmentally sustainable solution.

Grape skins, seeds, and stems are substrates rich in dietary fibers, comprising major constituents such as cellulose, hemicellulose, and lignin [17–19]. This composition prompts an evaluation of grape waste biochar as electrically conducting fillers, given that biochar derived from lignin and cellulose can achieve conductivities comparable to carbon black [20,21], a commonly used filler in antistatic composite materials. This enhanced conductivity arises from the high-carbon polyaromatic structure developed during pyrolysis, a property that, in some instances, was exploited to obtain graphene-like structures through post-modification [22].

Bipolar Plates (BPs) play a crucial role in ensuring the proper distribution of reactants and products during the operation of fuel cells and electrolyzers [23]. They are instrumental in both the production of clean hydrogen and its effective utilization. Compared to metallic BPs, graphite-based BPs offer notable advantages, including lower corrosion and reduced weight. While bulk graphite boasts exceptional electrical and thermal conductivity, as well as high chemical inertness, it does exhibit brittleness. This limitation can be addressed with composite BPs [24], composed of powdered graphite and an organic polymeric binder. High-filled composite BPs can retain most of the graphite's beneficial properties, achieving excellent in-plane electrical conductivities (IPCs) as required by the technical standards (>100 S/cm) [23].

In this study, the valorization of different winery byproducts, specifically woody stems (WSs), grape skins (GSs), whole grape seeds (WGSs), and defatted grape seeds (DGSs) were evaluated through biochar production. Two pyrolysis conditions were investigated, all conducted at a consistent temperature of 300 °C but varying in pyrolysis duration (3 h and 24 h). The

selection of these specific pyrolysis times was intended to thoroughly investigate the impact of thermal processing duration on the yield and properties of the resulting biochar. Slow pyrolysis, characterized by lower temperatures and extended processing times, generally leads to higher biochar yields [25]. By examining both shorter (3 h) and longer (24 h) durations, we aimed to assess how the composition of biochar evolves over pyrolysis times. The 3 h pyrolysis allows us to study the initial stages of biomass decomposition and biochar formation, corresponding to the minimum processing time (energy input), useful for industrial applications. Conversely, the 24 h pyrolysis process allows us to observe the effects of prolonged heat exposure on the final composition and quality of biochar. Longer pyrolysis times are expected to facilitate more complete carbonization, potentially enhancing electrical conductivity. The biochar samples were characterized by thermogravimetric (TG) analysis. Moreover, the obtained biochars were evaluated as a substitute for fossil graphite within composite BPs, potentially enhancing both its cost-effectiveness and sustainability by improving the renewable carbon footprint. The findings could contribute to the development of more environmentally friendly hydrogen economy while leveraging agricultural waste for valuable applications.

2. Materials and Methods

2.1. Chemicals

Diglycidylether of bisphenol A (DGEBA) resin DER 331[®] (187 g/eq) was purchased from Dow Chemicals (Midland, MI, USA); isophoronediamine (IPDA) hardener (42.57 g/eq) and dichloromethane (DCM) were purchased from Merck (Darmstadt, Germany); GraphCOND[®] 45/98 X, D50 75 mm, 98% carbon (G45) and GraphTERM[®] 23/99.9, D50 23 mm, 99.9% carbon (G23) were purchased from Georg H. LUH GmbH (Walluf, Germany); carbon black (CB) (PBX51) D50 17 mm was purchased from Cabot Corporation (Alpharetta, GA, USA).

2.2. Sample Preparation

Woody stems (WSs) of *Vitis vinifera* cultivar Grapa Rossa were collected from a farm in the Modena (Italy) area, alongside the grapes utilized for obtaining grape skin (GS) and whole grape seed (WGS) samples. Defatted grape seeds (DGSs) were sourced from Randi Group, a local company based in Faenza, Italy, specializing in grape seed oil production (<https://www.randi-group.com/it/randigroup/>, accessed on 14 February 2024). DGSs are derived from a blend of grape seeds collected from wineries across northern Italy, irrespective of cultivar or geographic origin. According to the company, DGSs constitute ~90% of the waste generated from grape seed oil production, consistent with findings from previous studies [26–28].

All samples were pre-dried in a laboratory oven (Argo LAB, Carpi, MO, Italy) (oven-dried samples, OD) to decrease moisture levels to below 8 wt%. This low moisture content contributes to the long-term stability of the matrices and inhibits the growth of mold and undesirable microorganisms.

Pyrolysis was conducted in a laboratory muffle under N₂ flow, carbonizing the samples at 300 °C for 3 and 24 h. Figure 1 presents the DGS samples pyrolyzed for 3 and 24 h, by way of example.



Figure 1. Defatted grape seed (DGS) samples pyrolyzed at 300 °C for 3 h (left) and 24 h (right).

2.3. Proximate Composition

The moisture and ash content were assessed following protocols recommended by the Association of Official Analytical Chemists [29]. The moisture content was determined by drying the samples at 105 °C until a constant weight was achieved. The ash content was determined using a laboratory furnace with a gradual temperature ramp up to 550 °C. Each measurement was performed in triplicate, and the results were averaged. CHN elemental analysis was conducted with a CHNS Analyzer Flash2000 (Thermo-Scientific, Waltham, MA, USA).

2.4. TGA

Thermogravimetric analysis was conducted using a Seiko SSC 5200 thermal analyzer (Seiko Instruments Inc., Chiba, Japan) under inert atmosphere conditions. The heating protocol employed a gradient of 10 °C /min over the temperature range of 25–1000 °C, with ultrapure helium purging at a flow rate of 100 µL/min.

2.5. Powder Preparation

All samples were prepared maintaining a fixed 85/15 filler-to-binder ratio [24]. In a 100 mL round-bottom glass flask, equipped with a magnetic stirring bar, CB, G23, G45, biochar, and DCM (35 mL) were introduced, and the suspension was stirred at 360 rpm for 5 min. Subsequently, DGEBA epoxy resin (0.56 g, dissolved in 2 mL of DCM) was added under stirring, and 2 min later, IPDA (0.12 g, dissolved in 2 mL of DCM) was slowly dropped under stirring. The mixture was further stirred for 5 min. Then, the solvent was removed via a rotary evaporator, resulting in 4.5 g of powder, which was divided into four replicates of approximately 1.0 g per sample. For each type of the obtained biochar samples (WSs, GSs, WGSs, and DGSs), six different loadings (wt%) were included within the BP formulations, as shown in Table 1. Additionally, two different pyrolysis conditions (3 h at 300 °C or 24 h at 300 °C) were evaluated.

Table 1. Compositions of biochar conductive samples.

| Biochar Loading (wt%) | Biochar (g) | G45 (g) | G23 (g) | CB (g) | DGEBA (g) | IPDA (g) |
|-----------------------|-------------|---------|---------|--------|-----------|----------|
| 10 | 0.46 | 2.65 | 0.57 | 0.19 | 0.56 | 0.12 |
| 15 | 0.68 | 2.47 | 0.54 | 0.18 | 0.56 | 0.12 |
| 20 | 0.91 | 2.29 | 0.50 | 0.17 | 0.56 | 0.12 |
| 25 | 1.14 | 2.12 | 0.46 | 0.16 | 0.56 | 0.12 |
| 30 | 1.37 | 1.94 | 0.42 | 0.14 | 0.56 | 0.12 |
| 35 | 1.59 | 1.77 | 0.38 | 0.13 | 0.56 | 0.12 |

2.6. Molding

Each dried powder sample (approximately 1.0 g) was pressed at 160 °C and 100 MPa for 12 min in a 2 cm i.d. mold. The obtained discs (see Figure 2), having a thickness close to 2 mm, were subsequently post-cured in oven at 60 °C for 48 h.



Figure 2. WS_3h prepared BP samples with biochar loading of 10 wt% (left) and 35 wt% (right).

2.7. In-Plane Conductivity (IPC) Measurements

IPC was measured by means of a digital sourcemeter (Keithley 2400 SMU, Keithley Instruments, Inc., Cleveland, OH, USA) equipped with a four-point probe, as described earlier [24]. Each sample was measured in 10 different points (five per side), and the mean IPC (S/cm) value was obtained as the inverse of the resistivity ρ ($\Omega \cdot \text{cm}$), as depicted in Equation (1). The mean resistivity value was corrected accordingly to the sample geometry, by means of the $F(t/s)$ factor of Equation (2), tabulated by F.M. Smits [30].

$$\text{IPC} = \frac{1}{\rho} \quad (1)$$

$$\rho = \left(\frac{\pi}{\ln 2} \cdot \frac{V}{I} \right) \cdot t \cdot F\left(\frac{t}{s}\right) \quad (2)$$

where V is the measured voltage (mV), I is the measured current (mA), t is the sample thickness (cm), and s is the spacing between two probes (cm).

2.8. Density Measurements

The density was calculated with standard weight/volume formula. Samples masses were measured with an analytical balance. The sample thickness was obtained as the mean value of four measurements carried out with a 0.01 mm resolution micrometer, while the samples' area was almost constant ($=3.141 \text{ cm}^2$) due to the mold's internal dimensions.

2.9. Statistical Analysis

The results are expressed as means \pm standard deviations of the mean and statistically analyzed using Matlab R2023a software. For comparison of the results, a one-way analysis of variance (ANOVA) test followed by a Tukey–Kramer post hoc ANOVA test was used, and p values of less than 0.05 were considered statistically significant. PCA analysis was carried out by using the PLS-Toolbox 2.1 for Matlab[®] (distributed by Eigenvector Research, Wenatchee, WA, USA).

3. Results

3.1. Proximate Composition

The geographical origin, degree of maturation, cultivar, and other factors exert a substantial and meaningful influence on the chemical composition of plant-based matrices [31,32]. In this study, proximate analysis offers a comprehensive insight into the variations in chemical composition of the matrices following the pyrolysis procedure. The results of the proximate analysis are reported in Table 2.

The data reported in Table 2 show an increase in carbon content (C %) and a decrease in the hydrogen (H %) and oxygen (O %) contents with pyrolysis time. Therefore, O/C and H/C ratios decreased accordingly. This trend is primarily attributed to the substantial loss of oxygenated and other functionalized compounds during heating, along with the release of VOCs and removal of inherent water. The observed increase in nitrogen content (N %) during pyrolysis can be attributed to several interrelated factors associated with the differential thermal stability and decomposition rates of various biomass components. Specifically, proteins exhibit a longer half-life compared to other components, reflecting their higher stability. Complete protein degradation during pyrolysis only occurs at temperatures above 500 °C; at lower temperatures, proteins are transformed into amines (through decarboxylation) or *N*-heterocycles [33,34] through Maillard reactions with sugars.

Thermochemical conversion of organic material involves numerous physical and chemical changes that yield solids (char), liquids, and gases, which may exhibit improved properties as materials or as fuels. Pyrolysis or carbonization, conducted in the absence of oxidants (e.g., oxygen), primarily result in the formation of solids as primary products. Slow pyrolysis is particularly effective for biochar production, typically yielding around 35% biochar from the dry biomass weight [7]. During heating, free moisture is

first lost, and from approximately 120 °C onward, the chemical bonds of primary biomass constituents—hemicellulose, cellulose, and lignin—are progressively rearranged, forming new functional groups (e.g., carboxyl, lactone, quinone, chromene, anhydride, phenol, ether, pyrone, pyridine, pyridone, and pyrrole) [7], and releasing VOCs [35]. These volatile matters include CO₂, CO, CH₄ [36], H₂O, and various condensable organic species under ambient conditions. The remaining carbon-rich, non-volatile solid residue of biomass is referred to as biochar. Biochar produced at low temperatures (300–400 °C) exhibits various oxygenated functional groups on its surface, derived from partial degradation of initial biopolymers. Conversely, biochar produced at higher temperatures (600–700 °C) exhibits a highly hydrophobic nature with well-organized carbon-rich layers reminiscent of graphite [37]. A lower O/C ratio enhances the stability of biochar, making it similar to carbon black [25]. The H/C ratio serves as an indicator of biochar structure; values below 0.1 suggest a high abundance of fused aromatic ring structures [38]. Biochar also retains a significant portion of the mineral matter originally present in the biomass, resulting in an increase in ash percentage content compared to the non-pyrolyzed samples.

Table 2. Proximate analysis of the oven-dried biomass samples, before and after pyrolysis.

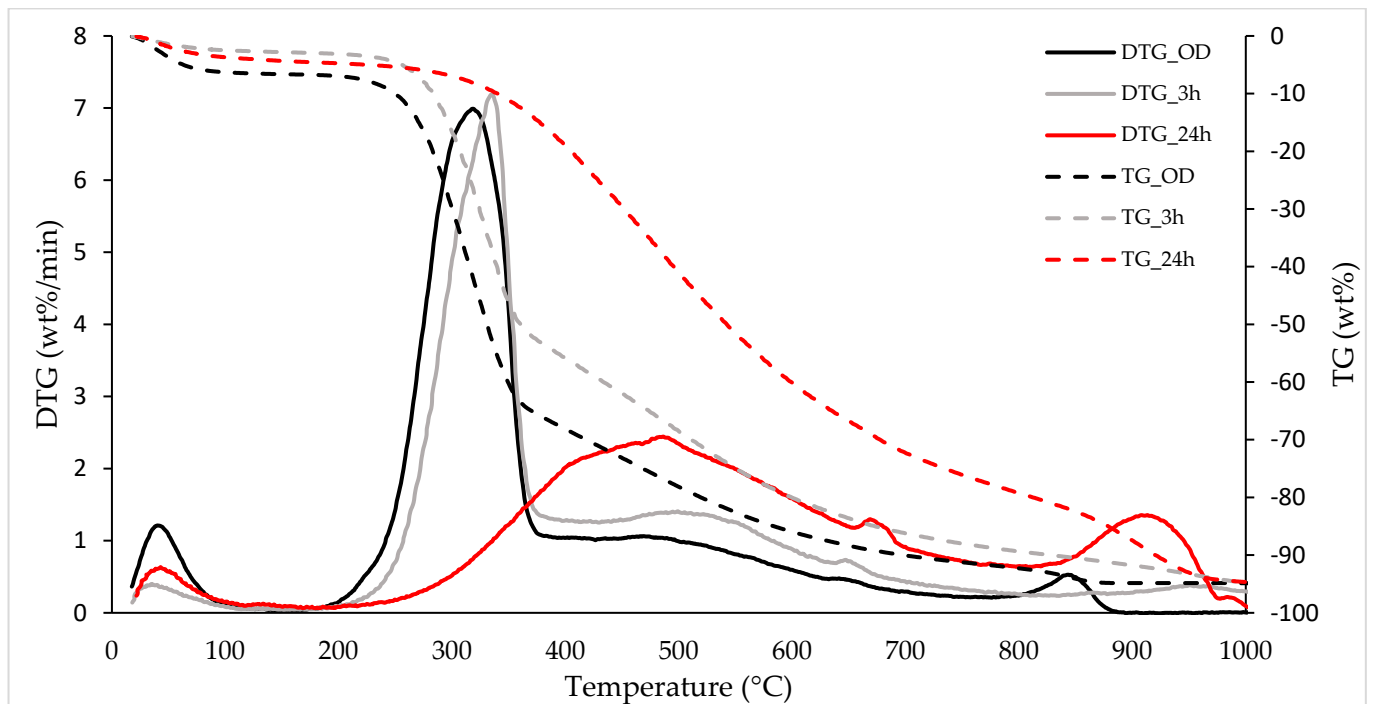
| | Pyrolysis Conditions | WSs | GSs | WGSs | DGSs |
|----------------------|----------------------|---------------------------|---------------------------|--------------------------|--------------------------|
| Moisture | - | 6.97 ± 0.04 ^{ab} | 6.89 ± 0.07 ^a | 6.12 ± 0.03 ^c | 7.06 ± 0.09 ^b |
| | 300 °C, 3 h | 2.47 ± 0.02 ^a | 2.56 ± 0.05 ^a | 1.01 ± 0.06 ^b | 0.97 ± 0.04 ^b |
| | 300 °C, 24 h | 2.44 ± 0.02 ^a | 2.60 ± 0.02 ^b | 1.03 ± 0.04 ^c | 1.04 ± 0.03 ^c |
| Ash | - | 3.07 ± 0.02 ^a | 5.71 ± 0.04 ^b | 3.13 ± 0.03 ^a | 2.07 ± 0.02 ^c |
| | 300 °C, 3 h | 3.68 ± 0.02 ^a | 6.65 ± 0.04 ^b | 3.55 ± 0.02 ^c | 2.94 ± 0.03 ^d |
| | 300 °C, 24 h | 4.23 ± 0.04 ^a | 7.61 ± 0.03 ^b | 3.71 ± 0.01 ^c | 3.44 ± 0.04 ^d |
| C | - | 45.0 ± 0.3 ^a | 47.2 ± 0.6 ^b | 51.5 ± 0.4 ^c | 51.2 ± 0.5 ^c |
| | 300 °C, 3 h | 51.0 ± 0.1 ^a | 57.8 ± 0.4 ^b | 63.9 ± 0.4 ^c | 58.9 ± 0.1 ^d |
| | 300 °C, 24 h | 61.7 ± 0.1 ^a | 63.1 ± 0.2 ^b | 68.8 ± 0.2 ^c | 64.9 ± 0.1 ^d |
| H | - | 6.99 ± 0.21 ^a | 6.72 ± 0.53 ^{ab} | 6.01 ± 0.31 ^b | 6.08 ± 0.11 ^b |
| | 300 °C, 3 h | 5.57 ± 0.14 ^a | 5.08 ± 0.01 ^b | 5.98 ± 0.15 ^c | 5.28 ± 0.02 ^b |
| | 300 °C, 24 h | 3.10 ± 0.04 ^a | 3.62 ± 0.03 ^b | 5.62 ± 0.02 ^c | 3.72 ± 0.07 ^b |
| N | - | 0.50 ± 0.05 ^a | 1.46 ± 0.08 ^b | 1.22 ± 0.02 ^c | 1.43 ± 0.07 ^b |
| | 300 °C, 3 h | 0.58 ^{*a} | 1.67 ± 0.05 ^b | 1.90 ± 0.36 ^b | 2.26 ± 0.39 ^b |
| | 300 °C, 24 h | 1.19 ± 0.03 ^a | 2.31 ± 0.01 ^b | 2.38 ± 0.03 ^b | 2.89 ± 0.15 ^c |
| S | - | <0.1 | <0.1 | <0.1 | <0.1 |
| | 300 °C, 3 h | <0.1 | <0.1 | <0.1 | <0.1 |
| | 300 °C, 24 h | <0.1 | <0.1 | <0.1 | <0.1 |
| O (by difference) | - | 44.4 ± 0.3 ^a | 38.9 ± 0.6 ^b | 38.1 ± 0.3 ^b | 39.2 ± 0.5 ^b |
| | 300 °C, 3 h | 39.2 ± 0.2 ^a | 28.8 ± 0.4 ^b | 24.7 ± 0.9 ^c | 30.6 ± 0.5 ^d |
| | 300 °C, 24 h | 29.8 ± 0.1 ^a | 23.4 ± 0.2 ^b | 19.5 ± 0.2 ^c | 25.0 ± 0.4 ^d |
| O/C | - | 0.99 | 0.82 | 0.74 | 0.77 |
| | 300 °C, 3 h | 0.77 | 0.50 | 0.39 | 0.52 |
| | 300 °C, 24 h | 0.48 | 0.37 | 0.28 | 0.39 |
| H/C | - | 0.16 | 0.14 | 0.12 | 0.12 |
| | 300 °C, 3 h | 0.11 | 0.09 | 0.09 | 0.09 |
| | 300 °C, 24 h | 0.05 | 0.06 | 0.08 | 0.06 |

Biomass was oven-dried before pyrolysis. Data are expressed as mean ± SD of three replicates; * SD < 0.01; ^{a,b,c,d} differences between means indicated by the same letter within the same row are not statistically significant ($p < 0.05$) according to the Tukey–Kramer HSD post hoc test.

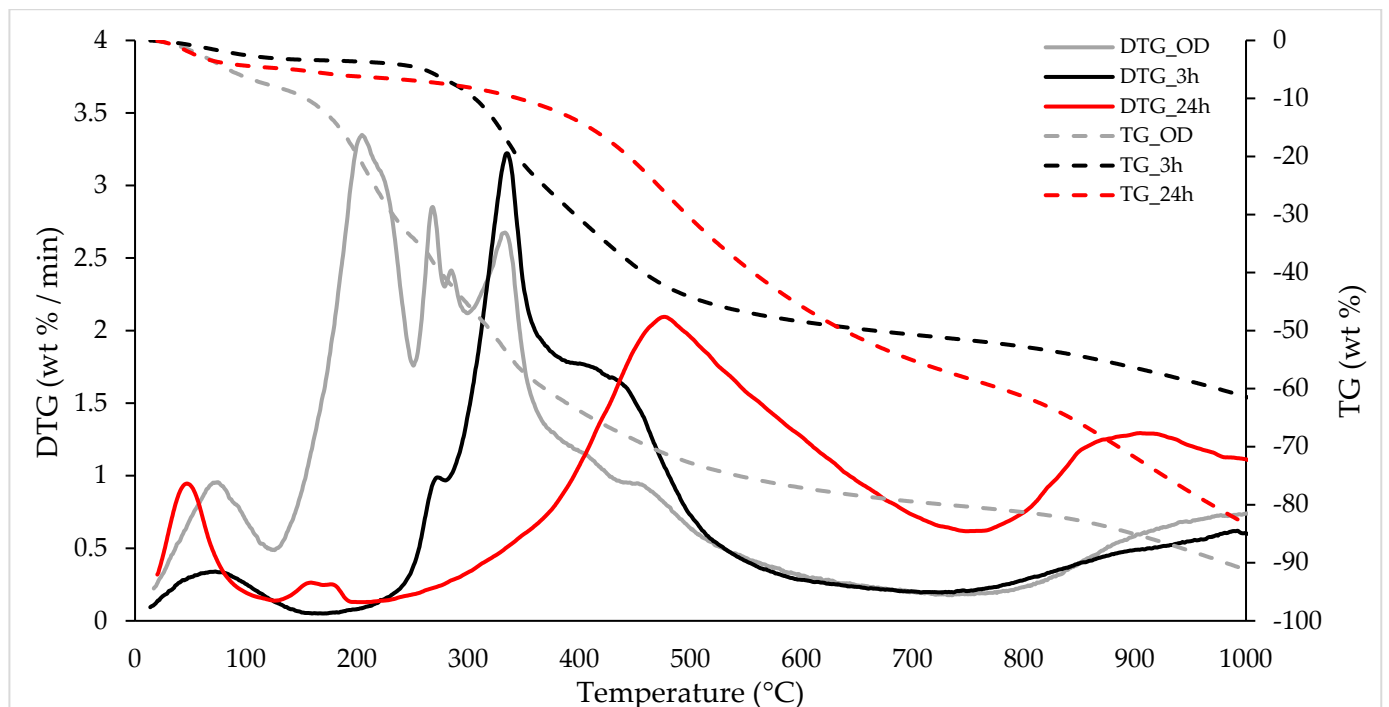
3.2. TGA

Each biomass constituent decomposes at different rates and within distinct temperature ranges. The TGA profiles of WS, GS, WGS and DGS samples at a 10 °C/min heating

rate are shown in Figure 3a–d, respectively. The TGA data are represented by the dashed lines, while the differential thermal gravimetric, DTG, and percentage mass losses are shown by solid lines and the percentage values on the left-hand scale.

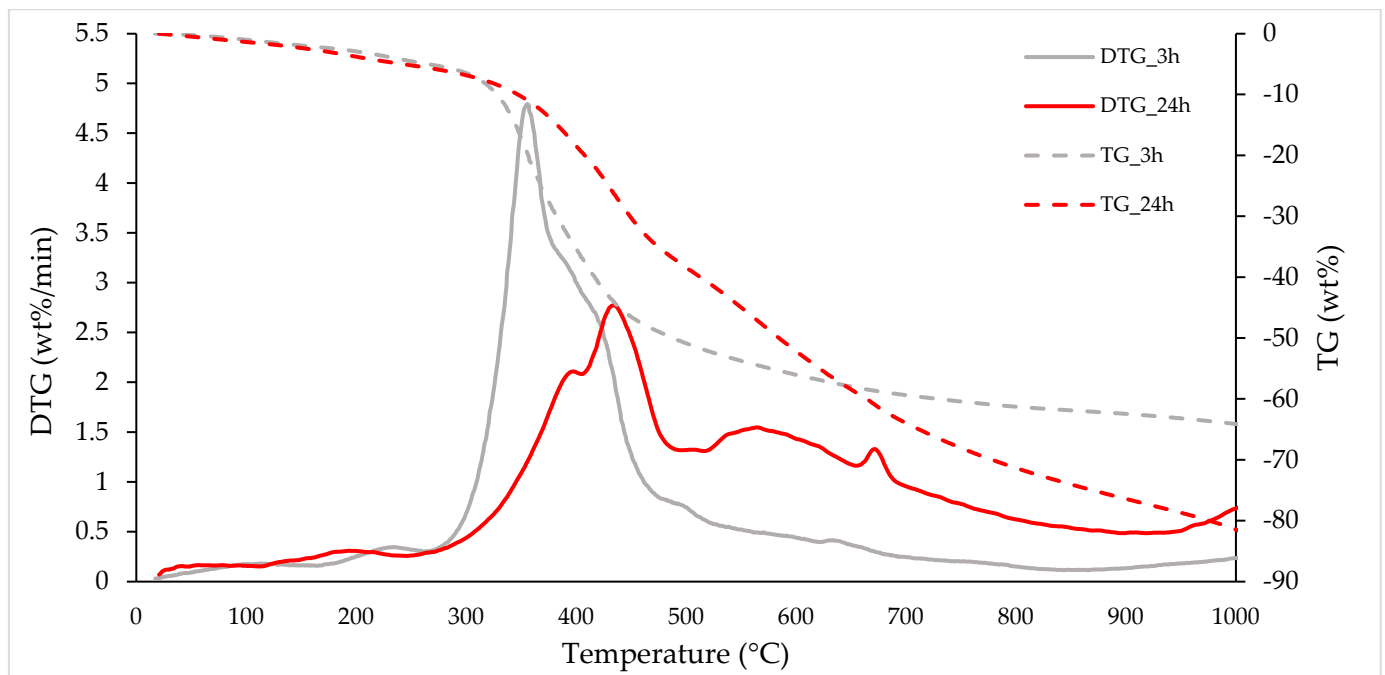


(a)

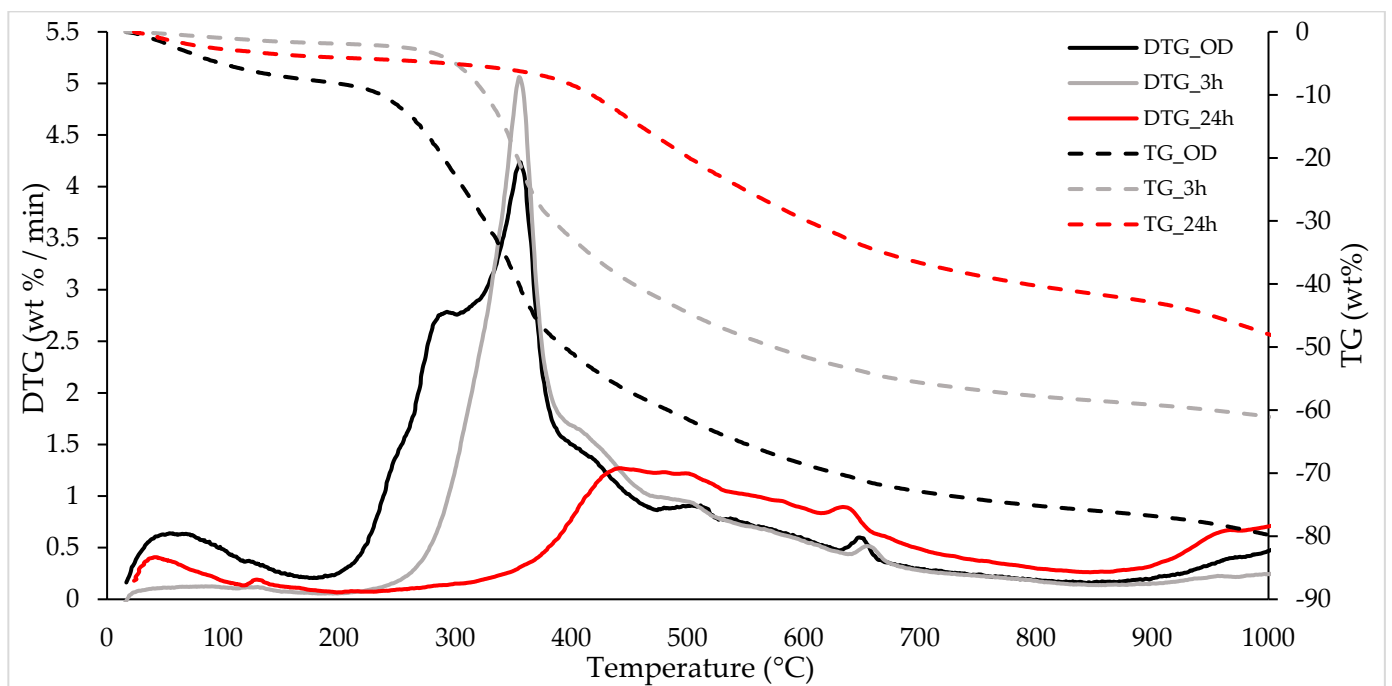


(b)

Figure 3. Cont.



(c)



(d)

Figure 3. TG (dashed lines) and DTG (solid lines) curves of the OD and pyrolyzed (for 3 or 24 h) WS (a), GS (b), WGS (c), and DGS (d) samples at a heating rate of 10 °C/min in helium atmosphere.

Table 3 summarizes the thermal degradation processes observed in the TGA/DTG profiles. This analysis provides information on the various degradative processes involving the main biomass constituents, such as hemicellulose, cellulose, lignin, proteins (2–15%) [28,31,39,40], and, in specific samples like WGSs, lipids (8–20%) [39,41,42]. These degradation processes can also occur simultaneously within specific temperature ranges, which are clearly identifiable in the thermograms of Figure 3. Comparing the TG and DTG profiles of non-pyrolyzed and pyrolyzed biomasses provides insights into the extent of degradation of their constituents.

Table 3. Thermally activated processes.

| Region | Thermally Activated Process |
|-------------|---|
| 20–120 °C | Removal of moisture and VOCs. |
| 120–250 °C | Removal of bound water, low-boiling VOCs, and caramelization of sugars. Degradation of pectin and proteins. |
| 250–400 °C | Degradation of hemicellulose, cellulose, and lipids. |
| 400–800 °C | Slow volatilization of lignin and volatilization of intermediate compounds formed after pyrolysis. |
| 800–1000 °C | Volatilization of carbon residues (C20–C40 fragments). |

The main volatilization fraction of the biomass took place between 200 and 400 °C for the oven-dried and 3 h pyrolyzed samples, while the samples pyrolyzed for 24 h showed a constant mass loss between 200 °C and 1000 °C. The significant release of VOCs can be attributed to the thermal decomposition of the three primary biomass constituents: hemicellulose, cellulose, and lignin.

The early mass losses observed in the DTG curves (Figure 3, temperature range of 30–120 °C) are attributed to the evaporation of moisture. As the treated samples were all pre-dried, the relative mass loss is limited (1–7%), with higher values for non-pyrolyzed samples. Some VOC loss also occurred within this temperature range.

In the temperature range of 120 °C to 250 °C, several thermal processes occur. Bound water, primarily associated with the inorganic fraction like mineral salts' crystallization water, and structural water, formed from condensation reactions of -OH groups in simple non-cellulosic carbohydrates, are removed. Moreover, semi-volatile compounds with medium-to-low vapor pressure (SVOCs), initially present or formed during heating, are completely eliminated. Thermal degradation of free amino acids begins around 180 °C, while proteins degrade more slowly, persisting up to 200–220 °C. Notably, the non-pyrolyzed GS sample (Figure 3b) exhibits significant mass loss (−34.0% at 250 °C), distinguishing it from other biomasses in this temperature region. This is mainly due to the degradation of pectin, which is absent in the WS, DGS, and WGS samples. Pectin typically presents two DTG signals, approximately at 200 and 230 °C, and is associated with decarboxylation and dehydration events in lateral chains [43–45].

The events occurring at higher temperatures (250–400 °C) are mainly attributed to the degradation of hemicelluloses and cellulose. Typically, hemicellulose degradation in an inert atmosphere occurs in the range of 220–315 °C [46–49], followed by the pyrolysis of cellulose (315–400 °C) [46–49]. These signals were observed in the DTG curves of OD and 3 h pyrolyzed samples. In the WS_OD sample (Figure 3a), a single broad peak extending from approximately 200 °C to 400 °C is observed, with a maximum at 318 °C. This peak likely includes the degradation of simple non-cellulosic carbohydrates, hemicelluloses, and cellulose. Accordingly, the mass loss relative to hemicellulose was absent in the WS_3h sample, as this biomass fraction was degraded during the thermal treatment (3 h at 300 °C), while the degradation of cellulose was still detectable (starting from ~230 °C and peaking at 335 °C). The DGS_3h sample (Figure 3d) is similar to WS_3h in this region, with a single peak in the DTG curve at 358 °C attributable to cellulose. However, the DGS_OD sample showed a different behavior, presenting a shoulder with a maximum rate of mass loss at 289 °C related to hemicelluloses, followed by a peak at 358 °C related to cellulose. The hemicellulose decomposition step often appears as a shoulder instead of a well-defined peak, a result that is in line with previous studies [48,50]. The GS samples (Figure 3b) showed two peaks in the DTG curves with maximum mass loss rates at 268 °C (GS_OD) and 272 °C (GS_3h), and 333 °C (GS_OD) and 335 °C (GS_3h), attributable to the degradation of hemicelluloses and cellulose, respectively. Additionally, the GS_OD sample showed a third small peak with a maximum loss rate at 285 °C, whose origin is unclear and requires further investigation. The absence of a clear distinction between the two peaks for hemicellulose and cellulose in the WS_OD sample indicates a higher hemicellulose content compared to the DGS and GS samples. The DTG curve of the WGS_3h sample (Figure 3c) showed a peak with a maximum at 355 °C, attributable to cellulose degradation. However, a shoulder emerged starting from approximately 380 °C and extending up to approximately 480 °C. A peak at 381 °C was linked to the degradation of unsaturated fatty acids by other authors [51].

Given the high content of unsaturated fatty acids in grape seeds [52], we can attribute this peak to their degradation. This signal is shifted at higher temperature (397 °C) in the WGS_24h sample. During extended pyrolysis, the breakdown of unsaturated fatty acids can result in the formation of intermediate compounds that may decompose at higher temperatures compared to the shorter pyrolysis duration.

Lignin, the first biomass constituent to undergo decomposition at lower temperatures, degrades slowly with a very low reaction rate extending throughout the pyrolysis process up to 800 °C. Its pyrolysis occurs over a broad temperature range due to the heterogeneous composition of lignin [53], leaving a higher residue at 1000 °C [49]. Significant lignin degradation occurs around 400 °C [46], marked by peaks or shoulders observed in the DTG curves of all analyzed samples. The main signal observed in all the samples pyrolyzed for 24 h up to 800 °C can be mainly attributed to the volatilization of the lignin fraction and other intermediate compounds formed after pyrolysis. In particular, depolymerization of hemicelluloses and celluloses leads to the formation of char residues that are stable up to 600–700 °C [49,54], while protein denaturation and degradation leads to the formation of *N*-heterocycles and nitriles, which are stable up to 800 °C [34].

Above 800 °C and up to the final temperature of 1000 °C, the residual stages of biomass degradation were observed. This temperature range represents the typical window for carbon pyrolysis, characterized by the thermal decomposition of low-volatile matter, including carbon fragments C₂₀–C₄₀, in the presence of mineral ashes. The total mass losses at 1000 °C vary among the samples, ranging from –48.9% for DGS_24h to –95.2% for WS_3h. For the GS and DGS samples pyrolyzed for 3 or 24 h, the mass loss at 1000 °C is significantly lower compared to their respective non-pyrolyzed samples. This can be attributed to the removal of VOCs and the formation of a more thermally stable char during the pyrolysis process. Additionally, the ash content of these pyrolyzed biomasses contributes to a lower mass loss at 1000 °C. In contrast, the WS samples showed a mass loss at 1000 °C of around 95% for all three samples, regardless of the pyrolysis process. This phenomenon can be attributed to several factors. The lower ash content in WS means that a greater proportion of the sample is composed of organic material that can decompose and volatilize at high temperatures. Additionally, the DTG curve of the WS_OD sample (Figure 3a) and some literature data indicated a higher content of hemicelluloses and cellulose in wood stems compared to grape skin and seeds [39,55–57], which typically leave less residue at 1000 °C [49].

3.3. Bipolar Plates

Several considerations are required to evaluate the use of biochar as a substitute for fossil graphite in the manufacture of composite BPs. Since the extraction and processing of fossil graphite are energy-intensive, it is essential to prefer biochars obtained through a low-energy pyrolysis process. This approach aligns with reducing carbon loss and corresponding CO₂ emissions, though it might impact the intrinsic electrical conductivity typically achieved during pyrolysis.

Several composite formulations including 10, 15, 20, 25, or 30 wt% of each of the available biochars (WSs, GSs, WGSs, and DGSs) were prepared, as shown in Table 1. Additionally, two alternative low-temperature pyrolysis conditions (300 °C for 3 h or 24 h) were considered. The obtained BP samples were then measured in terms of density (Table 4) and IPC (Table 5).

Table 4. Density values (g/cm³) of the BP samples.

| Sample | wt% | 10 | 15 | 20 | 25 | 30 | 35 |
|--------|-----|--------------------------|---------------------------|---------------------------|---------------------------|---------------------------|--------------------------|
| GS3 | | 1.78 ± 0.04 ^a | 1.72 ± 0.02 ^{ac} | 1.69 ± 0.04 ^{ac} | 1.62 ^{*ac} | | |
| WGS3 | | 1.59 ± 0.04 ^b | 1.56 ± 0.02 ^b | 1.53 ± 0.05 ^b | 1.49 ± 0.02 ^b | | |
| DGS3 | | 1.72 ± 0.07 ^a | 1.67 ± 0.02 ^a | 1.64 ± 0.03 ^{bc} | 1.57 ± 0.01 ^{bc} | 1.52 ± 0.07 ^a | 1.50 ± 0.01 ^a |
| WD3 | | 1.74 ± 0.04 ^a | 1.73 ± 0.03 ^{cd} | 1.70 ± 0.02 ^{cd} | 1.68 ± 0.02 ^{ad} | | |
| GS24 | | 1.77 ± 0.04 ^a | 1.74 ± 0.01 ^{cd} | 1.70 ± 0.03 ^{cd} | 1.64 ± 0.01 ^{ac} | | |
| WGS24 | | 1.74 ± 0.03 ^a | 1.71 ± 0.03 ^{ad} | 1.70 ± 0.01 ^{cd} | 1.66 ± 0.01 ^{ac} | 1.60 ± 0.01 ^{ab} | |
| DGS24 | | 1.84 ± 0.04 ^a | 1.77 ± 0.02 ^c | 1.75 ± 0.03 ^{ad} | 1.68 ± 0.01 ^{ad} | 1.64 ± 0.02 ^b | 1.57 ± 0.04 ^b |
| WD24 | | 1.82 ± 0.06 ^a | 1.76 ± 0.02 ^{cd} | 1.72 ± 0.06 ^{cd} | 1.64 ± 0.08 ^{ac} | | |

Data are expressed as mean ± standard deviation of three replicates; * SD < 0.01; ^{a,b,c,d} differences between means indicated by the same letters within the same column are not statistically significant ($p < 0.05$) according to the Tukey–Kramer HSD post hoc test.

Table 5. IPC values (S/cm) of the BP samples.

| Sample | wt% | 10 | 15 | 20 | 25 | 30 | 35 |
|--------|-----|----------------------------|---------------------------|---------------------------|---------------------------|---------------------------|--------------------------|
| GS3 | | 127.6 ± 9.6 ^{ab} | 113.1 ± 10.2 ^a | 96.7 ± 7.1 ^{abc} | 87.5 ± 8.8 ^{ab} | | |
| WGS3 | | 102.6 ± 11.4 ^a | 96.4 ± 7.2 ^a | 89.7 ± 8.7 ^{ac} | 73.5 ± 9.1 ^a | | |
| DGS3 | | 132.5 ± 10.1 ^b | 120.7 ± 9.9 ^a | 114.2 ± 8.1 ^{bc} | 95.4 ± 11.8 ^{ab} | 81.7 ± 10.6 ^{ab} | 74.4 ± 10.6 ^a |
| WD3 | | 120.5 ± 8.6 ^{ab} | 110.9 ± 11.7 ^a | 99.8 ± 6.2 ^{abc} | 89.4 ± 5.9 ^{ab} | | |
| GS24 | | 127.8 ± 9.6 ^{ab} | 114.2 ± 10.5 ^a | 94.1 ± 7.7 ^{abc} | 82.3 ± 11.5 ^{ab} | | |
| WGS24 | | 103.4 ± 9.9 ^a | 95.0 ± 10.3 ^a | 86.1 ± 7.2 ^a | 75.0 ± 8.9 ^{ab} | 66.6 ± 5.9 ^a | |
| DGS24 | | 128.7 ± 10.2 ^{ab} | 117.1 ± 10.6 ^a | 109.4 ± 8.7 ^c | 100.0 ± 10.0 ^b | 88.8 ± 8.5 ^b | 74.6 ± 9.9 ^a |
| WD24 | | 113.5 ± 9.6 ^{ab} | 104.2 ± 10.2 ^a | 96.2 ± 8.8 ^{abc} | 79.6 ± 6.9 ^{ab} | | |

Data are expressed as mean ± standard deviation of three replicates; ^{a,b,c} differences between means indicated by the same letters within the same column are not statistically significant ($p < 0.05$) according to the Tukey–Kramer HSD post hoc test.

Almost all composite samples featuring 10 wt% of biochar inclusion (first row of Tables 4 and 5) resulted in small deviations compared to the biochar-free reference (IPC = 153 S/cm; $d = 1.83$ g/cm³) [24]. This suggests that the biochar developed a respectable intrinsic conductivity. However, the inclusion of greater amounts of biochar resulted in progressively degraded performance in terms of both density and IPC. Densities values (Table 4) showed a much more pronounced influence from the pyrolysis time, presumably due to the relatively slow mass loss at 300 °C (see Figure 3). Overall, some interesting trends were evident from this study:

- Prolonged pyrolysis: Extending the pyrolysis duration from 3 h to 24 h provided only a small improvement in the intrinsic conductivity of the biochar. This indicates that the additional energy and time investment for longer pyrolysis may not yield substantial benefits in terms of electrical performance.
- Fat removal: The removal of fats from the grape seeds had a significant positive impact on the performance of the biochar. Defatted biochar (DGS3 and DGS24), compared to GS biochar, produced excellent composite materials, maintaining good performance even at higher biochar loadings. Specifically, composites with 25 wt% of DGS biochar (30 wt% of substituted G45 graphite) demonstrated superior results.
- Carbon content (C %): Biochars featuring higher carbon content (lower O/C ratio) such as DGS and GS (see Table 2) led to samples with higher IPC values, suggesting a higher intrinsic conductivity occurring in biochars with higher carbon content.

- Thermal stability: GS and DGS biochars exhibited higher thermal stability compared to WS samples, as shown by the relative TGA/DTG curves (Figure 3). Therefore, a higher degree of carbonization corresponds to a more stable structure.

4. Conclusions

The results of this study demonstrate that converting wine production waste into biochar through low-energy pyrolysis is a promising strategy to enhance the carbon neutrality of this activity. This option not only provides a simple way to retain most of the carbon present in the waste as biochar but also highlights its favorable application in the preparation of conductive composite materials suitable for BP manufacture. This, in turn, synergistically promotes the sustainable production (water electrolyzers) and use (fuel cells) of clean hydrogen.

These findings also provide a strong basis for further development. The TG analysis yielded valuable insights for interpreting the IPC values of the BP samples. Specifically, the pyrolyzed GS and DGS samples demonstrate enhanced thermal stability compared to their WS counterparts, along with higher IPC values. This greater thermal stability, indicative of a more graphite-like behavior, correlates positively with increased conductivity. Vegetable oil extraction is a low-energy input process and is highly desired for this application. After the separation of this valuable fraction, the resulting waste biomass can be easily processed through a short pyrolysis cycle (e.g., 3 h at 300 °C) to produce high-value biochar. The promising preliminary results for DGS biochar as a substitute for fossil graphite in conductive composite materials highlight the need for further research. By evaluating additional technical parameters such as hydrogen permeability and flexural strength, future studies can provide a more comprehensive understanding of the biochar-based composites' suitability for practical applications. This ongoing research will be crucial in optimizing the materials for performance, durability, and sustainability, thereby advancing the development of cleaner energy solutions.

Author Contributions: Conceptualization, F.R. and V.D.; methodology, V.D. and D.M.; software, V.D. and D.M.; validation, F.R., B.A. and A.L.; formal analysis, F.R., M.R. and V.D.; investigation, V.D., B.A., and A.L.; resources, F.R. and M.R.; data curation, V.D. and A.L.; writing—original draft preparation, V.D., M.R. and B.A.; writing—review and editing, F.R., D.M. and A.L.; visualization, V.D.; supervision, F.R. and M.R.; project administration, F.R. and M.R.; funding acquisition, F.R. All authors have read and agreed to the published version of the manuscript.

Funding: This research received no external funding.

Data Availability Statement: All data are contained within the article.

Acknowledgments: It is a pleasure to gratefully thank Giovanni Randi S.p.A. (Randi Group, Faenza, Italy) for providing us with the defatted grape seed (DGS) sample used in this article.

Conflicts of Interest: The authors declare no conflicts of interest.

References

1. FAOSTAT. Available online: <https://www.fao.org/faostat/en/#data> (accessed on 17 October 2022).
2. Jin, Q.; Wang, Z.; Feng, Y.; Kim, Y.-T.; Stewart, A.C.; O'Keefe, S.F.; Neilson, A.P.; He, Z.; Huang, H. Grape Pomace and Its Secondary Waste Management: Biochar Production for a Broad Range of Lead (Pb) Removal from Water. *Environ. Res.* **2020**, *186*, 109442. [CrossRef]
3. Beres, C.; Costa, G.N.S.; Cabezudo, I.; Da Silva-James, N.K.; Teles, A.S.C.; Cruz, A.P.G.; Mellinger-Silva, C.; Tonon, R.V.; Cabral, L.M.C.; Freitas, S.P. Towards Integral Utilization of Grape Pomace from Winemaking Process: A Review. *Waste Manag.* **2017**, *68*, 581–594. [CrossRef]
4. Devesa-Rey, R.; Vecino, X.; Varela-Alende, J.L.; Barral, M.T.; Cruz, J.M.; Moldes, A.B. Valorization of Winery Waste vs. the Costs of Not Recycling. *Waste Manag.* **2011**, *31*, 2327–2335. [CrossRef] [PubMed]
5. Gaunt, J.L.; Lehmann, J. Energy Balance and Emissions Associated with Biochar Sequestration and Pyrolysis Bioenergy Production. *Environ. Sci. Technol.* **2008**, *42*, 4152–4158. [CrossRef]
6. Li, Y.; Xing, B.; Ding, Y.; Han, X.; Wang, S. A Critical Review of the Production and Advanced Utilization of Biochar via Selective Pyrolysis of Lignocellulosic Biomass. *Bioresour. Technol.* **2020**, *312*, 123614. [CrossRef] [PubMed]

7. Tomczyk, A.; Sokołowska, Z.; Boguta, P. Biochar Physicochemical Properties: Pyrolysis Temperature and Feedstock Kind Effects. *Rev. Environ. Sci. Biotechnol.* **2020**, *19*, 191–215. [[CrossRef](#)]
8. Vaiškūnaitė, R.; Mažeikienė, A.; Mohammadi, K. Effects of Pyrolysis Temperature on Biochar Physicochemical and Microbial Properties for H₂S Removal from Biogas. *Sustainability* **2024**, *16*, 5424. [[CrossRef](#)]
9. Li, Y.; Gupta, R.; Zhang, Q.; You, S. Review of Biochar Production via Crop Residue Pyrolysis: Development and Perspectives. *Bioresour. Technol.* **2023**, *369*, 128423. [[CrossRef](#)] [[PubMed](#)]
10. Patzek, T.W.; Pimentel, D. Thermodynamics of Energy Production from Biomass. *Crit. Rev. Plant Sci.* **2005**, *24*, 327–364. [[CrossRef](#)]
11. Metzger, J.O. Production of Liquid Hydrocarbons from Biomass. *Angew. Chem. Int. Ed.* **2006**, *45*, 696–698. [[CrossRef](#)]
12. Kung, C.-C.; McCarl, B.A.; Cao, X. Economics of Pyrolysis-Based Energy Production and Biochar Utilization: A Case Study in Taiwan. *Energy Policy* **2013**, *60*, 317–323. [[CrossRef](#)]
13. Chan, K.Y.; Van Zwieten, L.; Meszaros, I.; Downie, A.; Joseph, S. Agronomic Values of Greenwaste Biochar as a Soil Amendment. *Soil Res.* **2007**, *45*, 629. [[CrossRef](#)]
14. Ding, W.; Dong, X.; Ime, I.M.; Gao, B.; Ma, L.Q. Pyrolytic Temperatures Impact Lead Sorption Mechanisms by Bagasse Biochars. *Chemosphere* **2014**, *105*, 68–74. [[CrossRef](#)] [[PubMed](#)]
15. Shen, Z.; Hou, D.; Jin, F.; Shi, J.; Fan, X.; Tsang, D.C.W.; Alessi, D.S. Effect of Production Temperature on Lead Removal Mechanisms by Rice Straw Biochars. *Sci. Total Environ.* **2019**, *655*, 751–758. [[CrossRef](#)] [[PubMed](#)]
16. Jia, M.; Wang, F.; Bian, Y.; Jin, X.; Song, Y.; Kengara, F.O.; Xu, R.; Jiang, X. Effects of pH and Metal Ions on Oxytetracycline Sorption to Maize-Straw-Derived Biochar. *Bioresour. Technol.* **2013**, *136*, 87–93. [[CrossRef](#)] [[PubMed](#)]
17. Venkitasamy, C.; Zhao, L.; Zhang, R.; Pan, Z. Grapes. In *Integrated Processing Technologies for Food and Agricultural By-Products*; Elsevier: Amsterdam, The Netherlands, 2019; pp. 133–163. ISBN 978-0-12-814138-0.
18. Deng, Q.; Penner, M.H.; Zhao, Y. Chemical Composition of Dietary Fiber and Polyphenols of Five Different Varieties of Wine Grape Pomace Skins. *Food Res. Int.* **2011**, *44*, 2712–2720. [[CrossRef](#)]
19. Barros, A.; Gironés-Vilaplana, A.; Texeira, A.; Baenas, N.; Domínguez-Perles, R. Grape Stems as a Source of Bioactive Compounds: Application towards Added-Value Commodities and Significance for Human Health. *Phytochem. Rev.* **2015**, *14*, 921–931. [[CrossRef](#)]
20. Kane, S.; Ulrich, R.; Harrington, A.; Stadie, N.P.; Ryan, C. Physical and Chemical Mechanisms That Influence the Electrical Conductivity of Lignin-Derived Biochar. *Carbon Trends* **2021**, *5*, 100088. [[CrossRef](#)]
21. Weber, K.; Quicker, P. Properties of Biochar. *Fuel* **2018**, *217*, 240–261. [[CrossRef](#)]
22. Plenča, K.; Cvetnić, S.; Prskalo, H.; Kovačić, M.; Cvetnić, M.; Kušić, H.; Matusinović, Z.; Kraljić Roković, M.; Genorio, B.; Lavrenčić Štangar, U.; et al. Biomass Pyrolysis-Derived Biochar: A Versatile Precursor for Graphene Synthesis. *Materials* **2023**, *16*, 7658. [[CrossRef](#)]
23. Jeong, K.I.; Oh, J.; Song, S.A.; Lee, D.; Lee, D.G.; Kim, S.S. A Review of Composite Bipolar Plates in Proton Exchange Membrane Fuel Cells: Electrical Properties and Gas Permeability. *Compos. Struct.* **2021**, *262*, 113617. [[CrossRef](#)]
24. Roncaglia, F.; Romagnoli, M.; Incudini, S.; Santini, E.; Imperato, M.; Spinelli, L.; Di Bona, A.; Biagi, R.; Mucci, A. Graphite-Epoxy Composites for Fuel-Cell Bipolar Plates: Wet vs Dry Mixing and Role of the Design of Experiment in the Optimization of Molding Parameters. *Int. J. Hydrogen Energy* **2021**, *46*, 4407–4416. [[CrossRef](#)]
25. Spokas, K.A. Review of the Stability of Biochar in Soils: Predictability of O:C Molar Ratios. *Carbon Manag.* **2010**, *1*, 289–303. [[CrossRef](#)]
26. Bordiga, M.; Travaglia, F.; Locatelli, M. Valorisation of Grape Pomace: An Approach That Is Increasingly Reaching Its Maturity—A Review. *Int. J. Food Sci. Technol.* **2019**, *54*, 933–942. [[CrossRef](#)]
27. Shinagawa, F.B.; Santana, F.C.D.; Torres, L.R.O.; Mancini-Filho, J. Grape Seed Oil: A Potential Functional Food? *Food Sci. Technol.* **2015**, *35*, 399–406. [[CrossRef](#)]
28. D'Eusanio, V.; Malferrari, D.; Marchetti, A.; Roncaglia, F.; Tassi, L. Waste By-Product of Grape Seed Oil Production: Chemical Characterization for Use as a Food and Feed Supplement. *Life* **2023**, *13*, 326. [[CrossRef](#)] [[PubMed](#)]
29. Association of Official Analytical Chemists. *AOAC Official Methods of Analysis of the Association of Official's Analytical Chemists*, 14th ed.; Association of Official Analytical Chemists: Washington, DC, USA, 1990; pp. 223–225+992–995.
30. Smits, F.M. Measurement of Sheet Resistivities with the Four-Point Probe. *Bell Syst. Tech. J.* **1958**, *37*, 711–718. [[CrossRef](#)]
31. D'Eusanio, V.; Genua, F.; Marchetti, A.; Morelli, L.; Tassi, L. Characterization of Some Stilbenoids Extracted from Two Cultivars of Lambrusco—Vitis Vinifera Species: An Opportunity to Valorize Pruning Canes for a More Sustainable Viticulture. *Molecules* **2023**, *28*, 4074. [[CrossRef](#)] [[PubMed](#)]
32. D'Eusanio, V.; Genua, F.; Marchetti, A.; Morelli, L.; Tassi, L. Exploring the Mineral Composition of Grapevine Canes for Wood Chip Applications in Alcoholic Beverage Production to Enhance Viticulture Sustainability. *Beverages* **2023**, *9*, 60. [[CrossRef](#)]
33. Chen, D.; Mei, J.; Li, H.; Li, Y.; Lu, M.; Ma, T.; Ma, Z. Combined Pretreatment with Torrefaction and Washing Using Torrefaction Liquid Products to Yield Upgraded Biomass and Pyrolysis Products. *Bioresour. Technol.* **2017**, *228*, 62–68. [[CrossRef](#)]
34. Leng, L.; Yang, L.; Chen, J.; Leng, S.; Li, H.; Li, H.; Yuan, X.; Zhou, W.; Huang, H. A Review on Pyrolysis of Protein-Rich Biomass: Nitrogen Transformation. *Bioresour. Technol.* **2020**, *315*, 123801. [[CrossRef](#)] [[PubMed](#)]
35. Neves, D.; Thunman, H.; Matos, A.; Tarelho, L.; Gómez-Barea, A. Characterization and Prediction of Biomass Pyrolysis Products. *Prog. Energy Combust. Sci.* **2011**, *37*, 611–630. [[CrossRef](#)]

36. Klason, K.T. Biochar Characterization and a Method for Estimating Biochar Quality from Proximate Analysis Results. *Biomass Bioenergy* **2017**, *96*, 50–58. [[CrossRef](#)]
37. Ahmad, M.; Rajapaksha, A.U.; Lim, J.E.; Zhang, M.; Bolan, N.; Mohan, D.; Vithanage, M.; Lee, S.S.; Ok, Y.S. Biochar as a Sorbent for Contaminant Management in Soil and Water: A Review. *Chemosphere* **2014**, *99*, 19–33. [[CrossRef](#)] [[PubMed](#)]
38. Leng, L.; Huang, H.; Li, H.; Li, J.; Zhou, W. Biochar Stability Assessment Methods: A Review. *Sci. Total Environ.* **2019**, *647*, 210–222. [[CrossRef](#)] [[PubMed](#)]
39. Spinei, M.; Oroian, M. The Potential of Grape Pomace Varieties as a Dietary Source of Pectic Substances. *Foods* **2021**, *10*, 867. [[CrossRef](#)] [[PubMed](#)]
40. Sagdic, O.; Ozturk, I.; Yetim, H.; Kayacier, A.; Dogan, M. Mineral Contents and Nutritive Values of the Pomaces of Commercial Turkish Grape (*Vitis vinifera* L.) Varieties. *Qual. Assur. Saf. Crops Foods* **2014**, *6*, 89–93. [[CrossRef](#)]
41. Rombaut, N.; Savoie, R.; Thomasset, B.; Castello, J.; Van Hecke, E.; Lanoisellé, J.-L. Optimization of Oil Yield and Oil Total Phenolic Content during Grape Seed Cold Screw Pressing. *Ind. Crops Prod.* **2015**, *63*, 26–33. [[CrossRef](#)]
42. Beveridge, T.H.J.; Girard, B.; Kopp, T.; Drover, J.C.G. Yield and Composition of Grape Seed Oils Extracted by Supercritical Carbon Dioxide and Petroleum Ether: Varietal Effects. *J. Agric. Food Chem.* **2005**, *53*, 1799–1804. [[CrossRef](#)]
43. Kozioł, A.; Środa-Pomianek, K.; Górnica, A.; Wikiera, A.; Cyprych, K.; Malik, M. Structural Determination of Pectins by Spectroscopy Methods. *Coatings* **2022**, *12*, 546. [[CrossRef](#)]
44. Einhorn-Stoll, U.; Kastner, H.; Fatouros, A.; Krähmer, A.; Kroh, L.W.; Drusch, S. Thermal Degradation of Citrus Pectin in Low-Moisture Environment—Investigation of Backbone Depolymerisation. *Food Hydrocoll.* **2020**, *107*, 105937. [[CrossRef](#)]
45. Zhou, S.; Xu, Y.; Wang, C.; Tian, Z. Pyrolysis Behavior of Pectin under the Conditions That Simulate Cigarette Smoking. *J. Anal. Appl. Pyrolysis* **2011**, *91*, 232–240. [[CrossRef](#)]
46. Díez, D.; Uruña, A.; Piñero, R.; Barrio, A.; Tamminen, T. Determination of Hemicellulose, Cellulose, and Lignin Content in Different Types of Biomasses by Thermogravimetric Analysis and Pseudocomponent Kinetic Model (TGA-PKM Method). *Processes* **2020**, *8*, 1048. [[CrossRef](#)]
47. Pardo, R.; Taboada-Ruiz, L.; Fuente, E.; Ruiz, B.; Díaz-Somoano, M.; Calvo, L.F.; Paniagua, S. Exploring the Potential of Conventional and Flash Pyrolysis Methods for the Valorisation of Grape Seed and Chestnut Shell Biomass from Agri-Food Industry Waste. *Biomass Bioenergy* **2023**, *177*, 106942. [[CrossRef](#)]
48. Khiari, B.; Jeguirim, M. Pyrolysis of Grape Marc from Tunisian Wine Industry: Feedstock Characterization, Thermal Degradation and Kinetic Analysis. *Energies* **2018**, *11*, 730. [[CrossRef](#)]
49. Yang, H.; Yan, R.; Chen, H.; Lee, D.H.; Zheng, C. Characteristics of Hemicellulose, Cellulose and Lignin Pyrolysis. *Fuel* **2007**, *86*, 1781–1788. [[CrossRef](#)]
50. Jeguirim, M.; Bikai, J.; Elmay, Y.; Limousy, L.; Njeugna, E. Thermal Characterization and Pyrolysis Kinetics of Tropical Biomass Feedstocks for Energy Recovery. *Energy Sustain. Dev.* **2014**, *23*, 188–193. [[CrossRef](#)]
51. Khalil, I.K.; Mustafa, A.S.; Mustafa, A.M. Study of Fatty Acid Composition, Physiochemical Properties and Thermal Stability of Broad Beans (*Vicia Faba*) Seed Oil. *Agric. Biol. J. N. Am.* **2017**, *8*, 141–146. [[CrossRef](#)]
52. Tangolar, S.G.; Özoğul, Y.; Tangolar, S.; Torun, A. Evaluation of Fatty Acid Profiles and Mineral Content of Grape Seed Oil of Some Grape Genotypes. *Int. J. Food Sci. Nutr.* **2009**, *60*, 32–39. [[CrossRef](#)]
53. Valente, M.; Brillard, A.; Schönnenbeck, C.; Brilhac, J.-F. Investigation of Grape Marc Combustion Using Thermogravimetric Analysis. Kinetic Modeling Using an Extended Independent Parallel Reaction (EIPR). *Fuel Process. Technol.* **2015**, *131*, 297–303. [[CrossRef](#)]
54. Shen, D.K.; Gu, S.; Bridgwater, A.V. The Thermal Performance of the Polysaccharides Extracted from Hardwood: Cellulose and Hemicellulose. *Carbohydr. Polym.* **2010**, *82*, 39–45. [[CrossRef](#)]
55. Prozil, S.O.; Evtuguin, D.V.; Lopes, L.P.C. Chemical Composition of Grape Stalks of *Vitis vinifera* L. from Red Grape Pomaces. *Ind. Crops Prod.* **2012**, *35*, 178–184. [[CrossRef](#)]
56. Mendes, J.A.S.; Xavier, A.M.R.B.; Evtuguin, D.V.; Lopes, L.P.C. Integrated Utilization of Grape Skins from White Grape Pomaces. *Ind. Crops Prod.* **2013**, *49*, 286–291. [[CrossRef](#)]
57. D'Eusario, V.; Morelli, L.; Marchetti, A.; Tassi, L. Aroma Profile of Grapevine Chips after Roasting: A Comparative Study of Sorbara and Spermola Cultivars for More Sustainable Oenological Production. *Separations* **2023**, *10*, 532. [[CrossRef](#)]

Disclaimer/Publisher's Note: The statements, opinions and data contained in all publications are solely those of the individual author(s) and contributor(s) and not of MDPI and/or the editor(s). MDPI and/or the editor(s) disclaim responsibility for any injury to people or property resulting from any ideas, methods, instructions or products referred to in the content.